EFFECTS OF REAR PLANFORM CROPPING CONFIGURATION ON WING-IN-GROUND CRAFT

Damian Raven Dewantara[1], I Ketut Aria Pria Utama[1*]

[1] Department of Naval Architecture, Institut Teknologi Sepuluh Nopember, Surabaya, Indonesia
E-mail: kutama@its.ac.id

Received: February 1, 2026 | **Accepted:** March 25, 2026 | **Published:** March 26, 2026
DOI: 10.12962/j27745449.v6i2.8361 | **Issue:** Volume 6 Number 2 2025 | **E-ISSN:** 2774-5449

ABSTRACT

Emissions from the global transportation sector represent a significant environmental challenge, with high-speed maritime transport being a notable contributor. The reduction of fuel consumption is therefore a critical objective in the development of future marine vehicles. The Wing-in-Ground (WIG) craft, an innovative transport modality developed since the mid-twentieth century, operates by utilising the aerodynamic ground effect to achieve aircraft-like speeds with substantially lower power requirements. This makes it a promising solution for efficient, high-speed maritime transit. A key innovation in WIG design is the Lippisch-style cropped reverse delta wing, a configuration known to enhance aerodynamic performance. To optimize this design, an investigation into the effects of rear planform cropping is required. This study employs computational fluid dynamics (CFD), utilising a Reynolds-Averaged Navier-Stokes (RANS) solver, to perform analysis of WIG models with various rear planform cropping configurations. The investigation covers trailing edge crop percentages of 0%, 10%, 20%, and 30% of the root chord. The results demonstrate that higher cropping percentages positively impact aerodynamic performance.

Keyword: wing-in-ground (WIG) craft, computational fluid dynamics, ground effect, transportation

Introduction

High-speed marine transport plays an important role in connecting offshore areas and archipelagos such as Indonesia and other regions in Southeast Asia. High-speed marine transport offers a cheaper alternative to air transport and is an important market.

Various innovations have been made to advance high-speed marine transport, such as the use of hydrofoils and hovercraft. An interesting development is the utilization of the ground effect in vehicles called wing-in-ground (WIG) Craft. The ground effect significantly increases the L/D ratio allowing for higher speeds with less required energy during flight. WIG Craft are shaped like aircraft with a design made to maximize the benefits of the ground effect, which is often most effective at altitudes within 25% of the wing's chord [1].

The ground effect increases lift by creating a high-pressure air cushion beneath the lifting object. The pressure caused by this air cushion is also known as ram pressure. The main parameter for this lift increase is the chord dominated ground effect, which is mainly caused by the ratio of height towards the wing's chord (h/c). On the other hand, the span dominated ground effect affects the reduction of drag. This is mainly affected by the ratio of height towards the wingspan. The span dominated ground effect causes a decrease in induced drag. Induced drag is caused by the formation of vortices at the wingtips. With the ground effect, the formation of these vortices is disrupted causing a decrease in induced drag [2].

Figure. 1 Airfish 8 WIG Craft [3]

Modern WIG Craft such as the Airfish-8 makes use of previous innovations, such as the reverse delta wing with anhedral. This design was pioneered by Alexander Lippisch in the mid-20th century [4]. An interesting addition to the wing configuration is the use of a rear planform cropping on the wing, as seen in Figure 1.

Previous research has provided valuable insights into the aerodynamics of these configurations. Lee & He [5] conducted experiments on various slender reverse delta wings outside of the ground effect, which concluded that the rear planform cropping resulted in a minor reduction in lift with a slight increase in drag. Within ground effect, Lee et al. [6] discovered that the addition cropping results in a higher lift. When a 30% cropped reverse delta wing was compared to the base non-cropped wing, the lift was higher. It was concluded to be caused by the wings smaller distance to the ground at a similar h/c ratio.

Unfortunately, there is a lack of studies that include the whole WIG model during the comparison of wing configurations. Thus, this research aims to address this gap by conducting analysis on various cropped reverse delta wing configurations on a full WIG Craft model. Through the use of ANSYS FLUENT CFD solver, this study aims to determine the effect of different rear planform cropping percentages on the craft's overall aerodynamic performance by observing lift and drag values.

Methodology

Model Geometry

The model geometry consists of the fuselage and wing. The fuselage is based on the existing Airfish-8 WIG Craft. Various percentages of rear planform cropping are applied to the wing model. The crop percentages tested are 0%, 10%, 20%, and 30% of the original root chord (12 m). The airfoil used for the wing section is the NACA 4412, while the NACA 0012 airfoil is used for the tail. Table 1 shows the wing data of each crop variation. Figure 2 shows the wing model design.

Table 1. Wing Data

Crop%	Wingspan	Tip Chord	Root Chord	Wing Area (m^2)	AR
0	10.8	2	12	75.6	1.543
10	10.8	2	10.8	74.8224	1.559
20	10.8	2	9.8	72.4896	1.609
30	10.8	2	8.4	68.6016	1.700

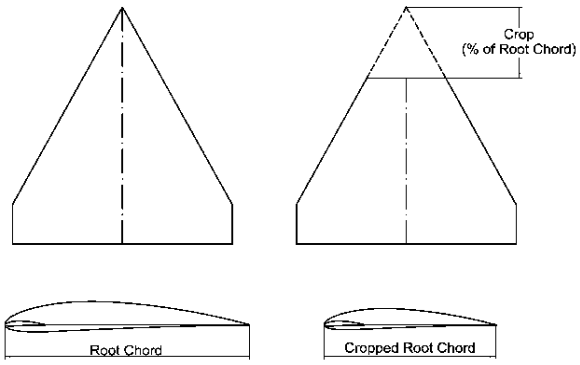

Figure 2. Cropped Wing Planform and Section

The wing is modelled first and then combined with the fuselage model, as seen figure 3.

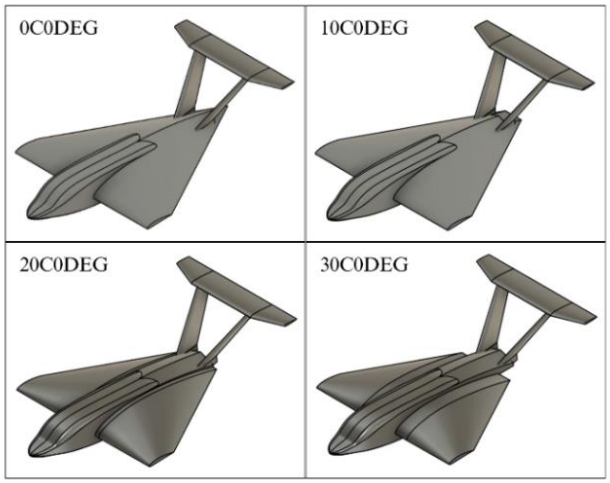

Figure. 3 WIG Variations

Domain and Boundaries

The simulation domain follows the guidelines set by the ITTC [7]. A reference length (L) is used to determine the distance from each boundary, here the root chord length (C) is used. The distance from the inlet used 10C and the outlet 20C, the width of the domain is set at a fixed value of 48 metres. Figure 4 show the domain size from the front and side.

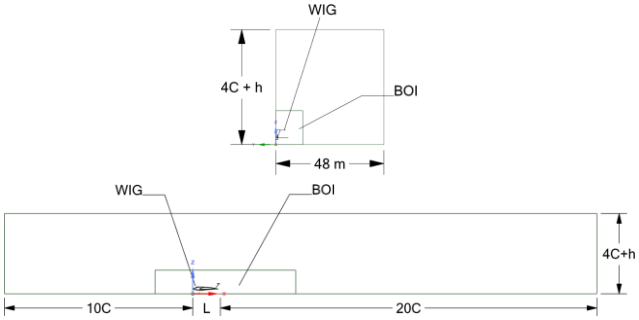

Figure 4. Domain size from the front (top) and the side (bottom)

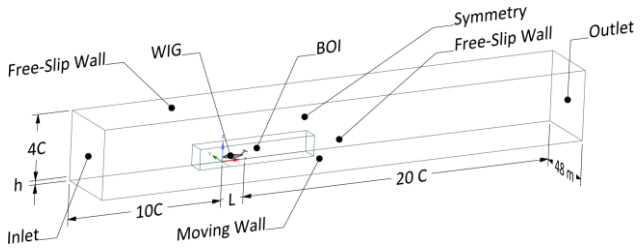

Figure 5. 3D Domain View

Figure 5 shows the boundary conditions used in the simulation. The velocity inlet is used with a velocity of 40 m/s, while the outlet type is set to a pressure outlet. To accurately represent the ground, a moving wall is used at the bottom with a velocity equal to the inlet velocity [8]. The side and top of the domain is set to a free-slip wall, so it does not interfere with the flow region. The WIG itself is set to a no-slip wall. A symmetry boundary is also used to reduce the number of elements in the grid and computational power required.

Governing Equations

The numerical solver used in this research is the academic version of ANSYS FLUENT 2023 R2. Incompressible steady viscous flow is used throughout the simulations. Reynolds-averaged Navier Stokes (RANS) equations are used to solve the flow. For incompressible and steady flow, the RANS equation for continuity and momentum are represented in equations (1) and (2) respectively [9].

$$\nabla \cdot \vec{V} = 0 \quad (1)$$

$$(\vec{V} \cdot \vec{\nabla})\vec{V} = -\frac{1}{\rho}\vec{\nabla}P' + \nu\nabla^2\vec{V} + \vec{\nabla} \cdot (\tau_{ij,turbulent}) \quad (2)$$

$$\tau_{ijt,turbulent} = \mu_t\left(\frac{\partial u_i}{\partial x_j} + \frac{\partial u_j}{\partial x_i}\right) - \frac{2}{3}\rho k\delta_{ij} \quad (3)$$

Here, $\tau_{ijt,turbulent}$ represents the Reynolds stresses. Using Boussinesq's hypothesis (equation 3) and the definition of the turbulent viscosity and turbulent kinetic energy, this term can be solved [10]. The turbulent viscosity and turbulent kinetic energy are defined manually based on a chosen turbulence model, which is selected in the CFD solver.

Solver Setup

Before the solver is set up, the model must go through the meshing process. The meshing process was done using ANSYS FLUENT MESHING, using the polyhedral shape for the volume mesh to support the complex geometry. Refinement was added around and behind the WIG model in order to accurately capture complex flow phenomena and the wake region. The number of elements used in this simulation is 6.79 million elements.

The turbulence model used in this work is the k-ω SST model, with an additional gamma-algebraic transition model. The k- ω SST model is known for its robustness for far from and near the wall through the use of a blending function [11]. The transition model allowed the solving of transition phenomenon on the WIG, such as the laminar separation bubble (LSB). The pressure-velocity coupling was handled with the SIMPLE algorithm, and second-order discretization schemes (QUICK for momentum and turbulence quantities, PRESTO! for pressure) were used to enhance solution accuracy and convergence.

In the simulations conducted in this work, the fluid properties are assumed to be consistent regardless of height. The properties of air are set to the default values, with a density of 1.225 kg/m^3 and a dynamic viscosity of 1.7894 x 10^{-5} kg/(m.s).

Results and Discussion

Grid Independence

To verify the results, verification is done through a grid independence study. Four grid variations are used for this study with the resulting lift coefficient (Cl) and drag coefficient (Cd) being compared. The results were shown to vary less as the number of elements increased as shown in Figure 6 and 7. As a result, the grid with 6.79 million elements was selected for further simulations.

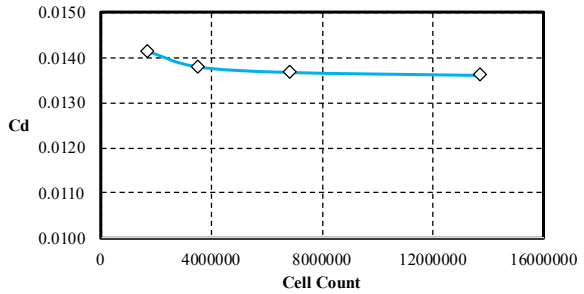

Figure 6. Grid Independence Results for Cd

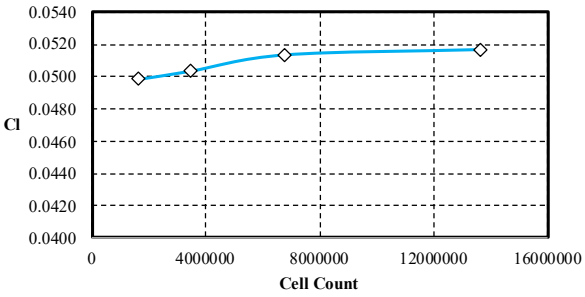

Figure 7. Grid Independence Results for Cl

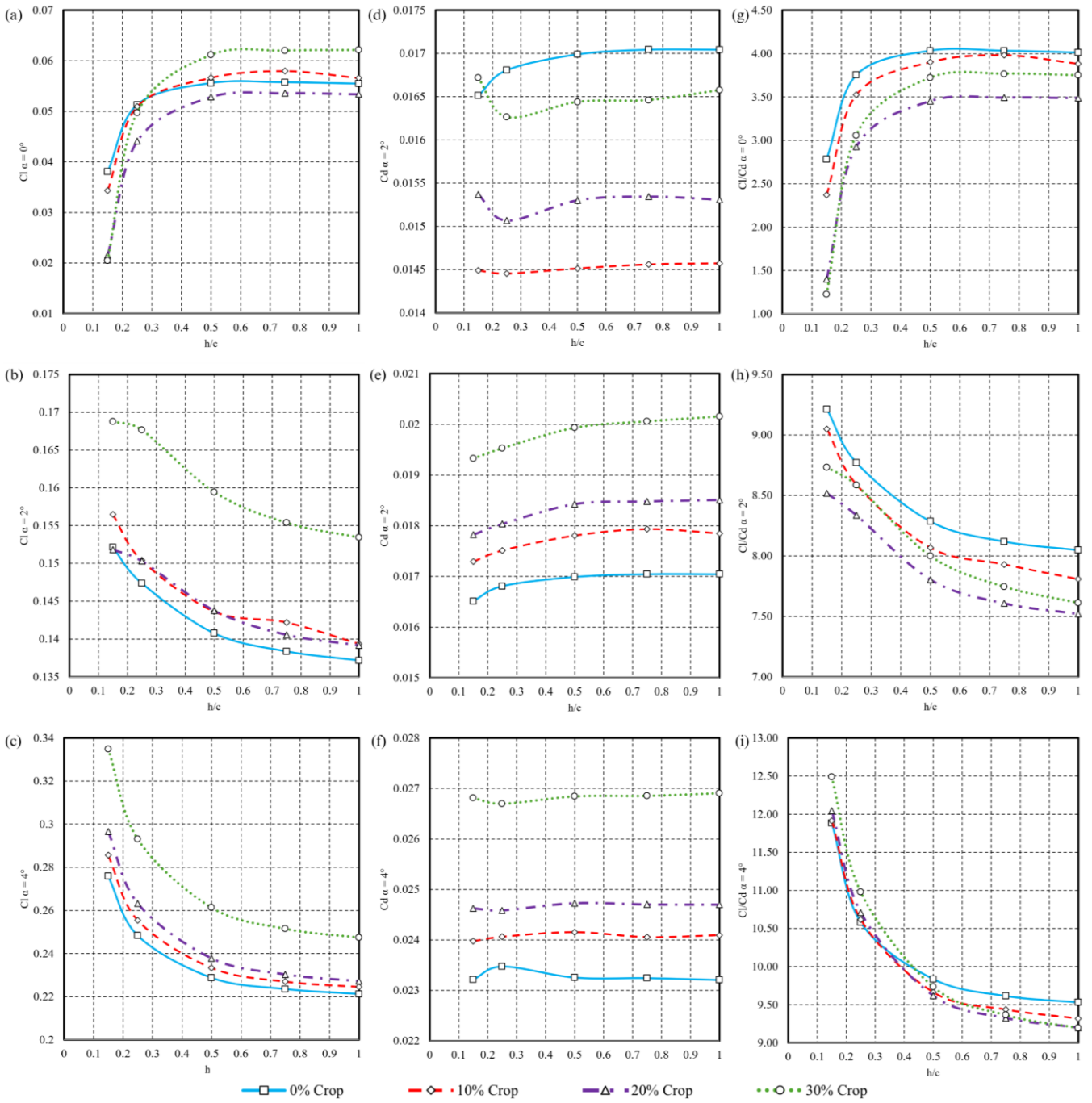

Figure 8. Simulation Results for (a) Cl at α = 0°, (b) α = 2°, and (c) α = 4°. (d) Cd at α = 0°, (e) α = 2°, and (f) α = 4°. (g) Cl/Cd at α = 0°, (h) α = 2°, and (i) α = 4°.

Lift and Drag Results

The results present the lift and drag coefficient results at various altitudes within ground effect and three angles of attack as seen in figure 8. These are presented separately and as the Cl/Cd ratio.

Figure 8 (a) shows the Cl at α = 0°, it can be observed that the lift decreases at a lower ground distance (h/c). The results at a positive angle of attack 2° (b) and 4° (c) contradict this and are more aligned with the principles of the ground effect, where lift increases with a higher ground proximity. The drag results show less variation across different heights, although there is a slight decrease in drag at a lower altitude. A small spike in the drag can be observed at α = 0° (d) across all crop variations except the uncropped wing. The angle of attack significant increase in the lift and drag, regardless of crop percentage. The drag at α = 2° (e) shows a consistent trend across all cropping variations, where the lower altitude results in a lower drag. At α = 4° (f), the drag fluctuates slightly for all variations. Very minimal difference for drag is observable for all heights.

A higher crop percentage causes a visible increase in lift and drags, but the 30% cropped wing shows the highest lift and drag across all heights and angles of attack except (d), with significant difference between other crop variations.

The Cl/Cd ratio show a small difference between the cropping variations, but the values trend similarly to the lift results. At α = 0° (Figure 8g) and α = 2° (Figure 8h), the highest Cl/Cd is produced from the base uncropped wing. At α = 4° (Figure 8i) and lower altitudes, higher crop percentages results in a higher Cl/Cd. Outside the ground effect, the highest Cl/Cd is produced from the uncropped wing.

Effect of Ground Proximity

While at positive angles of attack (α = 2° and α = 4°) the results align with existing theory about the ground effect, the results at a zero-degree angle of attack (α = 0°) contradict this. Usually, a higher proximity with the ground results in ram pressure, where the airflow is compressed in the gap between the WIG craft's lower surface and the ground, creating a high-pressure cushion that generates significant lift. However, at a α = 0° a powerful suction effect occurs. At α = 0◦, the geometry formed by the curved lower surface of the fuselage and the cambered NACA 4412 wing creates a convergent-divergent channel with the ground plane. This channel functions as a Venturi nozzle. As the airflow enters the constricted throat of this channel, it accelerates to a velocity significantly higher than the freestream velocity. In accordance with Bernoulli's principle, this region of high-velocity flow corresponds to a region of low static pressure on the craft's lower surface. This low-pressure zone, or suction, acts downward, directly counteracting the positive lift generated on the upper surfaces and leading to a loss of total lift.

Another term for this phenomenon is ‘flow blockage’ [12]. This condition occurs when the ground clearance is small, causing the developing boundary layers from both the wing's lower surface and the ground to interact. This interaction can establish a transient "fluid-throat," which leads to a condition known as external flow choking. The geometry formed between the wing and the ground acts as a temporary convergent-divergent nozzle as mentioned before, which significantly accelerates the airflow in the constricted space. This acceleration and subsequent choking can result in a sudden loss of lift. The phenomenon can also lead to the formation of shock waves, which generate additional turbulence and contribute to a sharp increase in pressure drag. This occurrence is also observed in various experiments regarding the ground effect. Lu et al. [13] experimented on a rectangular NACA 0012 wing and discovered that at α ≤ 3.5° the ground effect caused a smaller Cl compared to the wing out of ground effect due to the development of suction pressure. This phenomenon has also been reported for chambered airfoil such as the NACA 4412 in the experiment done by Ahmed et al. [14].

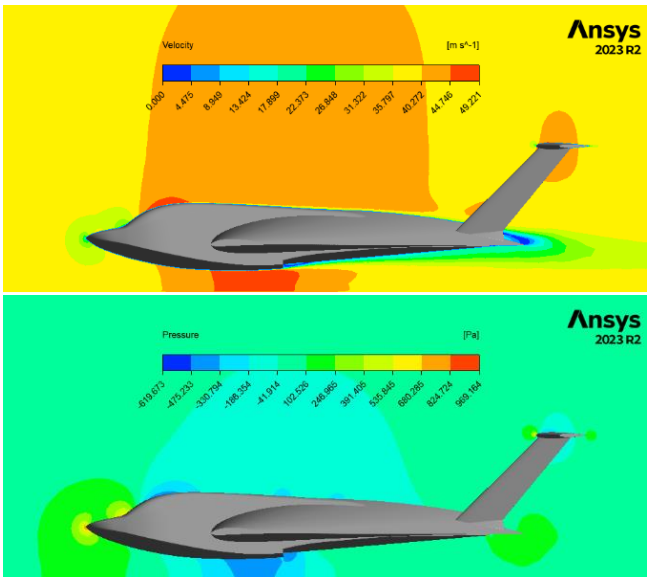

Figure 9. Contours of velocity (top) and pressure (bottom) at the symmetry for 10% crop variation, h/c = 0.15, α = 0°.

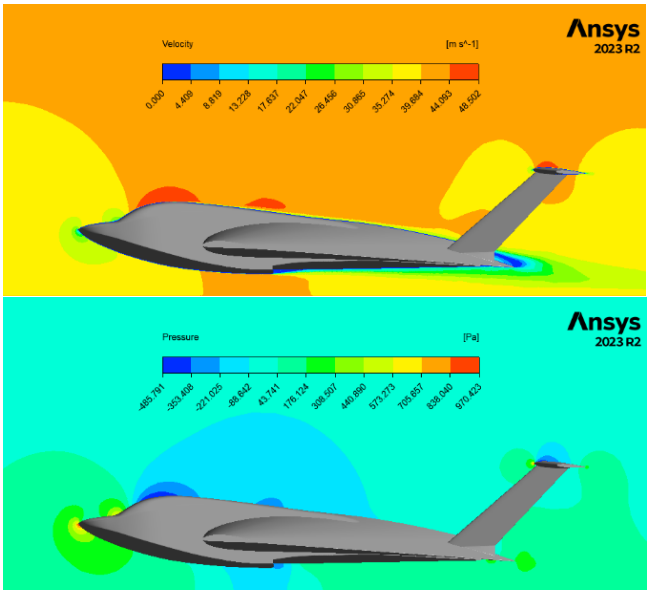

Figure 10. Contours of velocity (top) and pressure (bottom) at the symmetry for 10% crop variation, h/c = 0.15, α = 4°.

Figure 9 shows how the suction effect occurs at low altitudes at α = 0°. The small gap below the WIG craft causes an increase in velocity, represented by the red

area in the contour, which in turn causes a drop in pressure below the WIG, causing a major decrease in pressure. While the ground effect occurs at the bottom front region of the WIG, the suction at the middle region of the WIG defeats the benefits of the ground effect. Figure 10 displays the velocity and pressure contour at α = 4°. Here the suction effect still occurs but the drop in pressure is significantly smaller compared to the one that occurs at α = 0°. The pressure beneath the WIG is overall higher, especially in the front parts of the WIG leading to an increase in overall lift.

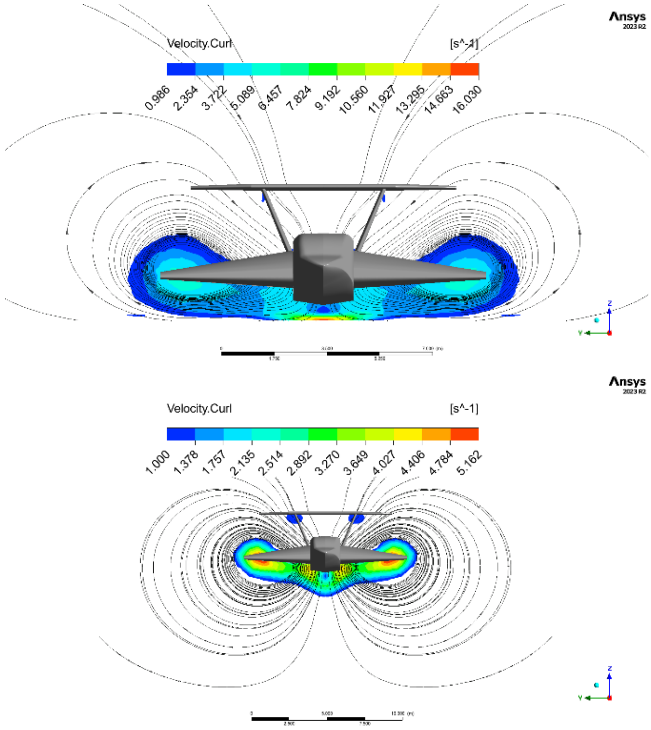

Figure 11. Vorticity contours and streamlines at h/c = 0.15 (top) and h/c = 1 (bottom) 18 m behind the leading edge for 10% crop variation, α = 2°.

While the suction effect disrupts the resulting lift, its effects toward drag are minimal as the drag is in accordance with the existing principles regarding the ground effect. The reduction in drag is caused by the disruption of vortex formation, which is the cause of induced drag, as visible in figure 11. There the formation of the vortices at the lower height (h/c = 0.15) is disrupted by the ground.

Effect Rear Planform Cropping

The analysis of rear planform cropping revealed it to be an effective method for enhancing aerodynamic performance within the ground effect. The results show that increasing the crop percentage leads to higher lift coefficients at positive angles of attack. The highest lift is achieved by the 30% cropped wing across all variations. The trailing edge portion of a reverse delta wing contributes minimally to lift generation while and contributes to friction drag. Cropping this aerodynamically inefficient section reduces both mass and drag. The definition of non-dimensional altitude (h/c) is based on the root chord (c). A WIG craft with a larger crop percentage has a smaller root chord. Therefore, at the same h/c value, the cropped craft is flying at a lower altitude (h) than its uncropped counterpart. This brings the WIG craft closer to the ground, increasing the strength of the ground effect.

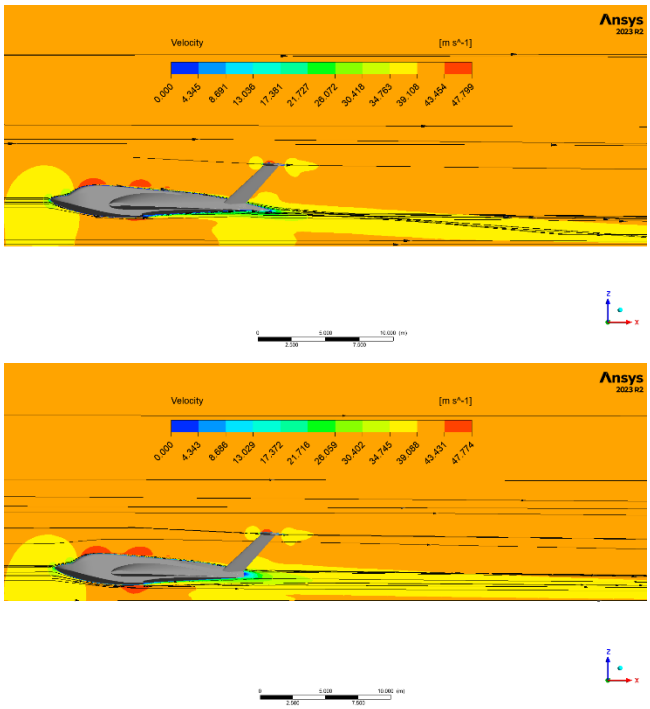

Figure 12. Wake region at 0% crop (top) and 30% crop (bottom) at h/c = 0.25 , α = 2°.

The drag, similar to the lift, also increases with the cropping percentage. The increase in drag is caused by the increasing pressure gradient due to the increase in lift. Another major contributing factor to the drag is due to interference drag, which is caused by the interaction between components of the WIG craft. Due to the fuselage being a fixed variable in this study, the shape of the fuselage does not change with the cropping percentage. Thus, the cropped section of the wing leaves a blunt part of the fuselage which also causes a large wake region behind the WIG craft as observable in figure 12. This additional wake causes an increase in drag as a result.

Across the Cl/Cd results, the lowest Cl/Cd is produced from the 20% crop variation, which is caused by the larger increase in drag compared to the lift. The base uncropped wing has the highest Cl/Cd at α = 0° and α = 2°, but at α = 4° and lower heights, the highest Cl/Cd

is achieved by the 30% cropped wing. This is due to the major increase of lift at lower heights. The higher drag in the cropped variations, either due to the suction effect or additional wake regions, causes it to be lower than the uncropped regions. Results show that at higher angles of attack will increase the effectiveness of rear planform cropping. At higher altitudes, where the influence of the ground effect is weaker, rear planform cropping effects performance negatively causing a decrease in lift and increasing drag.

Conclusion

This research has provided a close analysis of the aerodynamic performance of WIG craft with various rear-planform cropping configurations. Based on the results in can be concluded that:

- The highest lift is produced by the 30% cropped wing both within and outside of the ground effect. This is due to the closer proximity of the wing to the ground at an identical h/c compared to the other wings. Cropping also removes the small section of the trailing edge which gives minimal contribution towards lift, resulting in a higher Cl within the ground effect.
- Cropping results in a higher drag as well, as shown by the uncropped wing producing a lower drag at higher angles of attack. This is attributed to the higher pressure gradient due to the higher lift and the interference drag caused by the cropped wing. This explains the major difference in drag between the crop variations.
- At lower angles of attack, the highest Cl/Cd is achieved by the uncropped wing. At $\alpha = 4°$ and lowest altitudes, the highest Cl/Cd is produced by the cropped wings, especially the 30% cropped wing.

Acknowledgements

This research was financially supported by the Final Project Assistance Grant (Bantuan Tugas Akhir Mahasiswa) funded by Institut Teknologi Sepuluh Nopember (ITS) under the 2025 ITS Internal Research Grant Scheme contract number 2143/PKS/ITS/2025.

References

[1] K. V. Rozhdestvensky, *Aerodynamics of a Lifting System in Extreme Ground Effect*, Springer Berlin Heidelberg, 2000. DOI: https://doi.org/10.1007/978-3-662-04240-3.

[2] E. Cui and X. Zhang, *Ground Effect Aerodynamics*, in *Encyclopedia of Aerospace Engineering*, R. Blockley and W. Shyy (Eds.), Wiley, 2010. DOI: https://doi.org/10.1002/9780470686652.eae022.

[3] Wigetworks, *Wigetworks*, 2025. Available: https://wigetworks.com/ (accessed August 11, 2025).

[4] L. Yun, A. Bliault, and J. Doo, *WIG Craft and Ekranoplan: Ground Effect Craft Technology*, Springer, New York, 2010.

[5] T. Lee and S. M. He, *The Trailing Vortices Generated by a Reverse Delta Wing with Different Wing Configurations*, Aerospace Science and Technology, 82–83, 378–393 (2018). DOI: https://doi.org/10.1016/j.ast.2018.08.022.

[6] T. Lee, D. Huitema, and P. Leite, *Ground Effect on a Cropped Slender Reverse Delta Wing with Anhedral and Gurney Flaplike Side-Edge Strips*, Proceedings of the Institution of Mechanical Engineers, Part G: Journal of Aerospace Engineering, 233, 2433–2444 (2019). DOI: https://doi.org/10.1177/0954410018779504.

[7] ITTC, *Recommended Procedures and Guidelines: Practical Guidelines for Ship CFD Applications*, 7.5–03–02–03, ITTC, 2014.

[8] T. Barber, *Aerodynamic Ground Effect: A Case Study of the Integration of CFD and Experiments*, International Journal of Vehicle Design, 40, 299 (2006). DOI: https://doi.org/10.1504/IJVD.2006.009068.

[9] Y. A. Çengel and J. M. Cimbala, *Fluid Mechanics: Fundamentals and Applications*, McGraw-Hill Higher Education, 2006.

[10] ANSYS Inc., *ANSYS Fluent Theory Guide*, Release 2023 R2, Canonsburg, PA, 2023.

[11] F. R. Menter, *Two-Equation Eddy-Viscosity Turbulence Models for Engineering Applications*, AIAA Journal, 32, 1598–1605 (1994). DOI: https://doi.org/10.2514/3.12149.

[12] V. Sanal Kumar et al., *Phenomenological Introduction of Propulsion Aspect of External Flow Choking at Wing in Ground Effect*, 50th AIAA/ASME/SAE/ASEE Joint Propulsion Conference, American Institute of Aeronautics and Astronautics, 2014. DOI: https://doi.org/10.2514/6.2014-3772.

[13] [13] A. Lu, V. Tremblay-Dionne, and T. Lee, *Experimental Study of Aerodynamics and Wingtip Vortex of a Rectangular Wing in Flat Ground Effect*, Journal of Fluids Engineering, 141, 111108 (2019). DOI: https://doi.org/10.1115/1.4043593.

[14] M. R. Ahmed, T. Takasaki, and Y. Kohama, *Aerodynamics of a NACA4412 Airfoil in Ground Effect*, AIAA Journal, 45, 37–47 (2007). DOI: https://doi.org/10.2514/1.23872.